– Supplemental Material –
Signatures of a gearwheel quantum spin liquid in a spin-$\frac{1}{2}$ pyrochlore molybdate Heisenberg antiferromagnet

Yasir Iqbal,[1,*] Tobias Müller,[2] Kira Riedl,[3] Johannes Reuther,[4,5] Stephan Rachel,[6,7] Roser Valentí,[3] Michel J. P. Gingras,[8,9,10] Ronny Thomale,[2] and Harald O. Jeschke[11]

[1] *Department of Physics, Indian Institute of Technology Madras, Chennai, 600036, India*
[2] *Institute for Theoretical Physics and Astrophysics, Julius-Maximilian's University of Würzburg, Am Hubland, D-97074 Würzburg, Germany*
[3] *Institut für Theoretische Physik, Goethe-Universität Frankfurt, Max-von-Laue-Straße 1, D-60438 Frankfurt am Main, Germany*
[4] *Dahlem Center for Complex Quantum Systems and Fachbereich Physik, Freie Universität Berlin, D-14195 Berlin, Germany*
[5] *Helmholtz-Zentrum Berlin für Materialien und Energie, D-14109 Berlin, Germany*
[6] *School of Physics, The University of Melbourne, Parkville, VIC 3010, Australia*
[7] *Institut für Theoretische Physik, Technische Universität Dresden, D-01062 Dresden, Germany*
[8] *Perimeter Institute for Theoretical Physics, Waterloo, Ontario, Canada N2L 5G7*
[9] *Department of Physics and Astronomy, University of Waterloo, Waterloo, Ontario, Canada N2L 3G1*
[10] *Canadian Institute for Advanced Research, 180 Dundas Street West, Toronto, Ontario, Canada M5G 1Z8*
[11] *Research Institute for Interdisciplinary Science, Okayama University, 3-1-1 Tsushima-naka, Kita-ku, Okayama 700-8530, Japan*

Structure— We base our calculations on the $Lu_2Mo_2O_5N_2$ structure as determined by Clark *et al.* [S1] using powder neutron diffraction at $T = 4$ K. Both $48f$ and $8b$ positions of the pyrochlore structure are partially occupied by oxygen and nitrogen [see Fig. S1]. Rietveld refinement yielded O/N occupation numbers of 0.663/0.257 and 0.831/0.169 for the two Wyckoff positions. While the $8b$ occupations add to one, the refinement indicates slight O/N deficiency on $48f$. It is easily determined that ideal occupations of $48f$ providing a 5:2 oxygen to nitrogen ratio would be 0.6948/0.3052. In our calculations, we neglect the possible O/N deficiency and adopt these ideal occupations of the $48f$ position. Furthermore, we model the random O/N occupation of $48f$ and $8b$ sites using the virtual crystal approximation [S2]. This means that we assign nuclear charges of $Z = 7.6948$ and $Z = 7.831$ to $48f$ and $8b$, respectively.

Electronic structure— We perform electronic structure calculations for $Lu_2Mo_2O_5N_2$ using the full potential local orbital (FPLO) code [S4] using the generalized gradient approximation (GGA) functional in its Perdew-Burke-Ernzerhof (PBE) form [S5]. We correct for the strong correlations on the Mo^{5+} $4d$ orbitals using the GGA+U method [S6]. Fig. S2 shows the electronic structure for a ferromagnetic solution calculated with GGA+U. The Hund's rule coupling is fixed at a value of $J_{\rm H} = 0.6$ eV, which is typical for $4d$ transition metal ions. The onsite interaction is chosen to be $U = 2.5$ eV because the Heisenberg Hamiltonian parameters estimated at this value yield a Curie-Weiss temperature which is close to the experimentally observed value $\Theta_{\rm CW} = -121(1)$ K. There are many bands as the primitive cell contains two formula units of $Lu_2Mo_2O_5N_2$. Per Mo^{5+} ion, there is one occupied band of $4d$ character in the majority channel ($\uparrow$), corresponding to a magnetic moment of precisely $S = 1/2$. The narrow bands around -2 eV are the occupied Lu $4f$ states. The other occupied bands are O/N $2p$. At this value of U, $Lu_2Mo_2O_5N_2$ is a semiconductor with a small gap of $E_g = 0.15$ eV.

Exchange couplings— Next, we calculate the total energies for 25 different spin configurations of a $3 \times 1 \times 1$ supercell of the primitive cell of $Lu_2Mo_2O_5N_2$. An exam-

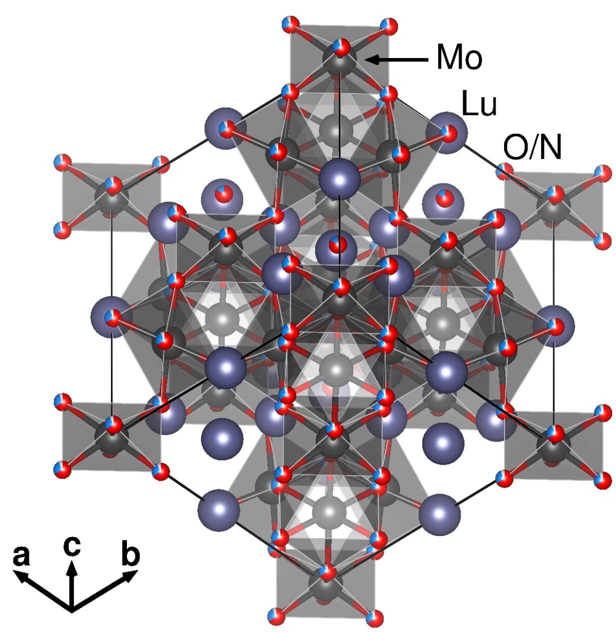

FIG. S1. Structure of $Lu_2Mo_2O_5N_2$. Note that sites partially occupied by oxygen and nitrogen are shown by partly red, partly blue balls.

U (eV)	J_1 (K)	J_2 (K)	J_{3a} (K)	J_{3b} (K)	J_5 (K)	Θ_{CW} (K)
2	102.4(6)	−0.1(5)	23.2(5)	−7.8(4)	−1.4(2)	−168(5)
2.25	88.1(6)	0.5(4)	19.9(4)	−6.6(4)	−1.1(2)	−147(5)
2.5	**74.8(5)**	**0.6(4)**	**17.2(4)**	**−5.8(3)**	**−0.99(11)**	**−125(4)**
2.75	62.0(5)	0.6(3)	15.0(4)	−5.2(3)	−0.89(10)	−104(3)
3	49.8(5)	0.6(4)	13.2(4)	−4.8(3)	−0.81(11)	−84(4)
3.25	37.8(5)	0.6(4)	11.7(4)	−4.6(4)	−0.74(11)	−65(4)
3.5	26.0(6)	0.6(4)	10.4(4)	−4.4(4)	−0.69(13)	−46(4)
3.75	14.2(6)	0.5(5)	9.3(5)	−4.5(4)	−0.64(14)	−26(4)

TABLE S1. Exchange coupling constants for the oxynitride phase $Lu_2Mo_2O_5N_2$ determined from total energies of 25 spin configurations in a 3×1×1 supercell using an 8×8×8 **k**-mesh [see Fig. 1 of main paper]. The parameters corresponding to $U = 2.5$ eV (marked in bold) are used for the PFFRG simulations. We adopt the convention in which each pair $\langle i, j\rangle$ in the summation in the exchange Hamiltonian [Eq. (1)] is counted only once. Accordingly, the formula for the Curie-Weiss temperature is $\Theta_{CW} = -\frac{1}{3}S(S+1)\sum_n z_n J_n$, where the summation extends over all neighbors with which a given spin interacts, and z_n is the coordination number at the nth-nearest-neighbor [S3].

ple for this procedure is illustrated in Fig. S3. We obtain the estimates for the Heisenberg exchange parameters listed in Table S1 by fitting the DFT+U total energies against the classical energies of the Heisenberg Hamiltonian. The evolution of exchange couplings with onsite interaction U is shown in Fig. 2. While the next nearest neighbor coupling J_2 is negligibly small, the two inequivalent third neighbor couplings J_{3a} (connecting two Mo^{5+} sites with with a nearest neighbor in between) and J_{3b} (across an empty hexagon in one of the three interpenetrating kagome lattices of the pyrochlore structure) are substantial and of different sign; J_{3a} is antiferromagnetic like J_1, and J_{3b} is ferromagnetic. We do not expect exchange couplings at Mo-Mo distances of 8 Å or more to play a major role. The $3 \times 1 \times 1$ supercell does not allow us to resolve J_4 ($d_{Mo-Mo} = 8.02$ Å) but we can determine J_5 ($d_{Mo-Mo} = 9.49$ Å) and find it to be very small. We derived the anisotropic exchange couplings in the framework of a combination of relativistic DFT calculations with exact diagonalization of a generalized Hubbard Hamiltonian on finite clusters, detailed in Ref. [S7]. Note that U in this method does not enter in the same way as in the GGA+U total energy calculations. We obtain the estimate of $|D|/J$ by scanning U values of up to 3.6 eV and values of the Hund's rule coupling J_H in the range of 0.6 eV to 0.8 eV.

Pseudofermion FRG— The PFFRG scheme [S8–S13] is a non-perturbative framework capable of handling arbitrary two-body spin-interactions of both diagonal and off-diagonal type [S14, S15], with any given

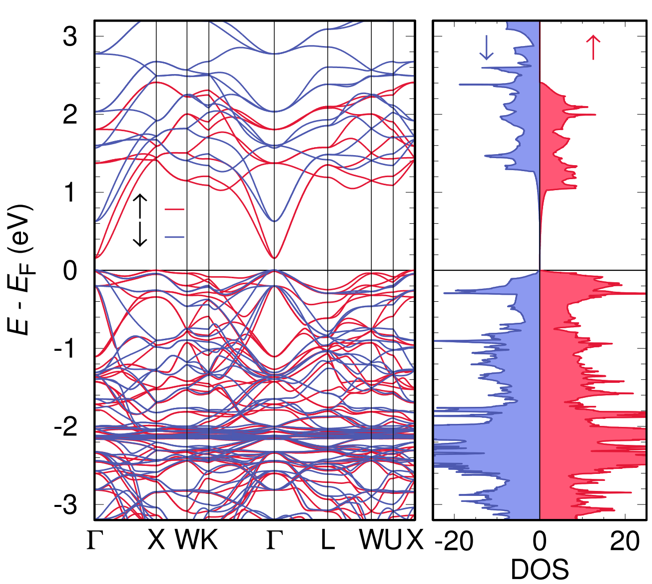

FIG. S2. Band structure and density of states of $Lu_2Mo_2O_5N_2$ calculated with GGA+U functional at $U = 2.5$ eV and $J_H = 0.6$ eV for the ferromagnetic state.

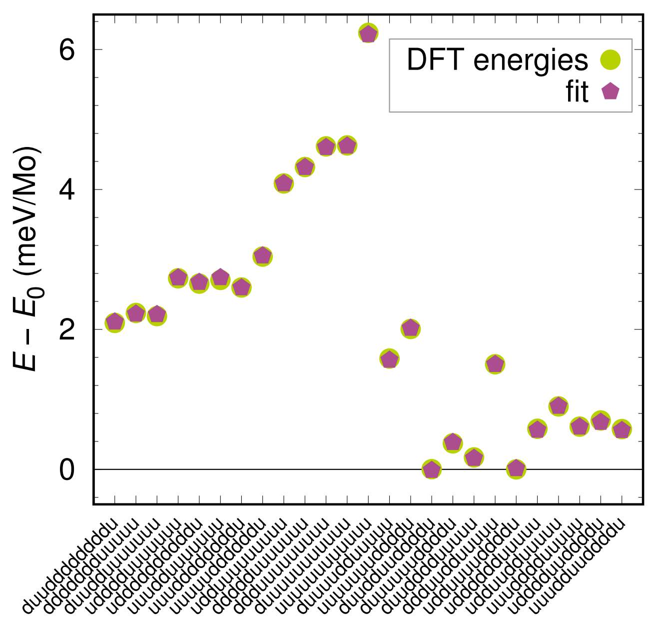

FIG. S3. Example for a set of 25 spin configurations of the considered $3 \times 1 \times 1$ supercell calculated with GGA+U functional at $U = 2.5$ eV and $J_H = 0.6$ eV. The quality of the fit to the Heisenberg model is very good.

spin [S16]. It is formulated in the SU(2) fermionic representation of spins, which amounts to rewriting the physical spin operator at each site in terms of Abrikosov pseudofermions,

$$\hat{\mathbf{S}}_i = \frac{1}{2}\sum_{\alpha,\beta} \hat{f}^{\dagger}_{i,\alpha}\boldsymbol{\sigma}_{\alpha\beta}\hat{f}_{i,\beta} \; , \tag{S1}$$

where α, $\beta =\uparrow$ or $\downarrow$, and $\hat{f}^{\dagger}_{i,\alpha}$ ($\hat{f}_{i,\alpha}$) are the pseudofermion creation (annihilation) operators, and $\boldsymbol{\sigma}$ is the vector of Pauli matrices. The fermionic representation is endowed with an enlarged Hilbert space which includes the unphysical *empty* and *doubly*-occupied sites carrying zero-spin, and must be projected out to restore the original Hilbert space of the Heisenberg model which has one-fermion-per-site. One way to achieve this is to add on-site level repulsion terms $-A\sum_i \mathbf{S}_i^2$ to the Hamiltonian, where A is a positive constant [S16]. Such terms lower the energy of the physical states but do not effect the unphysical ones. As a consequence, at sufficiently large A the low energy degrees of freedom of H are entirely within the physical sector of the Hilbert space. For a wide class of spin systems (including the models considered here) one finds that even for $A = 0$, the ground state of the fermionic Hamiltonian obeys the one-fermion-per-site constraint [S16]. This is because unphysical occupations effectively act like a vacancy in the spin lattice, and are associated with a finite excitation energy of the order of the exchange couplings. As a consequence, the ground state of the fermionic system is identical to the ground state of the original spin model where each site is singly occupied.

Within PFFRG, a step-like infrared frequency cutoff Λ along the Matsubara frequency axis is introduced in the bare fermion propagator $G_0(i\omega) = \frac{1}{i\omega}$, i.e., $G_0(i\omega)$ is replaced by

$$G_0^{\Lambda}(i\omega) = \frac{\Theta(|\omega| - \Lambda)}{i\omega} \; . \tag{S2}$$

Implanting this modification into the generating functional of the one-particle irreducible vertex function and taking the derivative with respect to Λ yields an exact but infinite hierarchy of coupled flow equations for the m-particle vertex functions [S17], which constitutes the FRG ansatz. The first two equations for the self energy Σ^{Λ} and the two-particle vertex Γ^{Λ} have the forms

$$\frac{d}{d\Lambda}\Sigma^{\Lambda}(1';1) = -\frac{1}{2\pi}\sum_{2'\,2}\Gamma^{\Lambda}(1',2';1,2)\,S^{\Lambda}(2,2') \tag{S3}$$

and

$$\begin{aligned}\frac{d}{d\Lambda}\Gamma^{\Lambda}(1',2';1,2) = {} & \frac{1}{2\pi}\sum_{3'\,3}\Gamma_3^{\Lambda}(1',2',3';1,2,3)\,S^{\Lambda}(3,3') \\ & +\frac{1}{2\pi}\sum_{3'\,3\,4'\,4}\Big[\Gamma^{\Lambda}(1',2';3,4)\,\Gamma^{\Lambda}(3',4';1,2) \\ & -\Gamma^{\Lambda}(1',4';1,3)\Gamma^{\Lambda}(3',2';4,2) - (3'\leftrightarrow 4', 3\leftrightarrow 4) \\ & +\Gamma^{\Lambda}(2',4';1,3)\Gamma^{\Lambda}(3',1';4,2) + (3'\leftrightarrow 4', 3\leftrightarrow 4)\Big] \\ & \times G^{\Lambda}(3,3')S^{\Lambda}(4,4') \; ,\end{aligned} \tag{S4}$$

where Γ_3^{Λ} denotes the three-particle vertex. Here, G^{Λ} is the fully dressed propagator and S^{Λ} is the so-called single scale propagator defined by

$$S^{\Lambda} = G^{\Lambda}\frac{d}{d\Lambda}\left[G_0^{\Lambda}\right]^{-1}G^{\Lambda} \; . \tag{S5}$$

Note that the arguments $1, 2, \ldots$ of the vertex functions and propagators denote multi indices "$1 \equiv \{\omega_1, i_1, \alpha_1\}$" containing the frequency variable ω_1, the site index i_1 and the spin index α_1.

For a numerical solution, this hierarchy of equations is truncated to keep only the self-energy Σ^{Λ} and two-particle vertex Γ^{Λ}. Particularly, the truncation on Γ_3^{Λ} is performed such that, via self-constistent feedback of the self-energy into the two-particle vertex, the approach remains separately exact in the large S limit as well as in the large N limit [where the spins' symmetry group is promoted from SU(2) to SU(N)] [S16]. While the terms representing the large S limit [second line of Eq. (S4)] describe the long-range ordering in classical magnetic phases, the large N terms [fourth line of Eq. (S4)] characterize the system with respect to non-magnetic resonating valence bond or dimer crystal phases. This allows for an unbiased investigation of the competition between magnetic ordering tendencies and quantum paramagnetic behavior. Approximations due to the neglect of the three-particle vertex Γ_3^{Λ} concern subleading orders in $1/S$ and $1/N$. Such terms are essential for probing possible chiral correlations in paramagnetic phases, e.g., in chiral spin liquids with a scalar chiral order parameters of the form $\sim \langle(\mathbf{S}_i \times \mathbf{S}_j)\cdot\mathbf{S}_k\rangle$. Therefore, the current implementation of the PFFRG does not allow to describe the possibility of a spin system to form chiral spin liquids.

The two-particle vertex in real space is related to the static spin-spin correlator

$$\chi_{ij}^{\mu\nu} = \int_0^{\infty} d\tau \langle \hat{S}_i^{\mu}(\tau)\hat{S}_j^{\nu}(0)\rangle \tag{S6}$$

where $\hat{S}_i^{\mu}(\tau) = e^{\tau\hat{\mathcal{H}}}\hat{S}_i^{\mu}e^{-\tau\hat{\mathcal{H}}}$. As a finite-size approximation, correlators $\chi_{ij}^{\mu\nu}$ are only calculated up to a maximal separation between sites i and j. The main physical outcome of the PFFRG are the Fourier-transformed correlators, i.e., the static susceptibility $\chi^{\mu\nu,\Lambda}(\mathbf{k})$ evaluated as a function of the RG scale Λ, which in three dimensions (for a $S = 1/2$ system) is related to a temperature $T = (\frac{\pi}{2})\Lambda$ [S18]. In our case, the maximal distance of the correlators is ~ 11.5 lattice spacings corresponding to a total volume of 2315 correlated sites which ensures a proper $\mathbf{k}$-space resolution. We implement an approach in which despite spatially limited vertices the system size is assumed to be, in principle, infinitely large. The frequency dependence of the two-particle vertex function is discretized over 64 points. If a system develops magnetic order, the corresponding two-particle vertex channel anomalously grows upon decreasing Λ and eventually causes the flow to become unstable. Otherwise, a smooth flow behavior of the susceptibility down to $\Lambda \to 0$ signals the absence of magnetic order.

Iterative minimization of the classical Hamiltonian— The ground state of a classical Heisenberg Hamiltonian is found using an iterative minimization scheme which preserves the fixed spin length constraint at every site [S19]. In contrast, within the Luttinger-Tisza method the fixed spin length constraint is only enforced globally, i.e., $\sum_i |\mathbf{S}_i^2| = S^2 N$, where N is the total number of lattice sites, implying that local moment fluctuations which are now permissible take us beyond the classical approximation by approximately incorporating some aspects of the quantum Hamiltonian [S20]. Starting from a random spin configuration on a lattice with periodic boundary conditions, we choose a random lattice point and rotate its spin to point antiparallel to its local field defined by

$$\mathbf{h}_i = \frac{\partial H}{\partial \mathbf{S}_i} = \sum_{j \neq i} J_{ij} \mathbf{S}_j. \tag{S7}$$

This results in the energy being minimized for every spin update and thereby converging to a local minimum. We choose a lattice with $L = 32$ cubic unit cells in each direction, and thus a single iteration consists of $16L^3$ sequential single spin updates. This iterative scheme is repeated many times starting from different random initial configurations to maximize the likelihood of having found a global minimum. From the minimal energy spin configuration, the spin structure factor

$$\mathcal{F}(\mathbf{k}) = \frac{1}{16L^3} \left| \sum_i \mathbf{S}_i e^{\imath \mathbf{k} \cdot \mathbf{r}_i} \right|^2 \tag{S8}$$

is computed.

* yiqbal@physics.iitm.ac.in

[S1] L. Clark, G. J. Nilsen, E. Kermarrec, G. Ehlers, K. S. Knight, A. Harrison, J. P. Attfield, and B. D. Gaulin, Phys. Rev. Lett. **113**, 117201 (2014).

[S2] L. Bellaiche and D. Vanderbilt, Phys. Rev. B **61**, 7877 (2000).

[S3] D. I. Khomskii, *Basic Aspects of the Quantum Theory of Solids. Order and Elementary Excitations* (Cambridge University Press, Cambridge, 2010).

[S4] K. Koepernik and H. Eschrig, Phys. Rev. B **59**, 1743 (1999).

[S5] J. P. Perdew, K. Burke, and M. Ernzerhof, Phys. Rev. Lett. **77**, 3865 (1996).

[S6] A. I. Liechtenstein, V. I. Anisimov, and J. Zaanen, Phys. Rev. B **52**, R5467 (1995).

[S7] K. Riedl, D. Guterding, H. O. Jeschke, M. J. P. Gingras, and R. Valentí, Phys. Rev. B **94**, 014410 (2016).

[S8] J. Reuther and P. Wölfle, Phys. Rev. B **81**, 144410 (2010).

[S9] J. Reuther and R. Thomale, Phys. Rev. B **83**, 024402 (2011).

[S10] J. Reuther, D. A. Abanin, and R. Thomale, Phys. Rev. B **84**, 014417 (2011).

[S11] J. Reuther, P. Wölfle, R. Darradi, W. Brenig, M. Arlego, and J. Richter, Phys. Rev. B **83**, 064416 (2011).

[S12] J. Reuther, R. Thomale, and S. Trebst, Phys. Rev. B **84**, 100406 (2011).

[S13] J. Reuther, R. Thomale, and S. Rachel, Phys. Rev. B **90**, 100405 (2014).

[S14] Y. Iqbal, P. Ghosh, R. Narayanan, B. Kumar, J. Reuther, and R. Thomale, Phys. Rev. B **94**, 224403 (2016).

[S15] M. Hering and J. Reuther, Phys. Rev. B **95**, 054418 (2017).

[S16] M. L. Baez and J. Reuther, Phys. Rev. B **96**, 045144 (2017).

[S17] W. Metzner, M. Salmhofer, C. Honerkamp, V. Meden, and K. Schönhammer, Rev. Mod. Phys. **84**, 299 (2012).

[S18] Y. Iqbal, R. Thomale, F. Parisen Toldin, S. Rachel, and J. Reuther, Phys. Rev. B **94**, 140408 (2016).

[S19] M. F. Lapa and C. L. Henley, ArXiv e-prints (2012), arXiv:1210.6810 [cond-mat.str-el].

[S20] I. Kimchi and A. Vishwanath, Phys. Rev. B **89**, 014414 (2014).